NILU Norsk institutt for luftforskning
Norwegian Institute for Air Research

Rotational Raman scattering in the O₂-A and O₂-B bands: Simulations for Carbonsat, FLEX/FLORIS, MERIS and OLCI

Arve Kylling

Scientific report

Generic Radiative Transfer Model for the Earth's
Surface-Atmosphere System: ESAS-Light II

ESTEC Contract No. AO/1-6607/10/NL/LvH

WP 2.2:

Rotational Raman scattering in the O_2-A and O_2-B bands: Simulations for CarbonSat, FLEX/FLORIS, MERIS and OLCI

Arve Kylling

NILU-Norwegian Institute for Air Research

Kjeller, Norway

March 5, 2012

1 Introduction

Rotational Raman scattering (RRS) causes filling-in of absorption lines in Earth shine spectra. It is routinely accounted for in analysis of UV and visible spectra measured both by satellite and ground-based instruments. RRS is also present at longer wavelengths, however, the magnitude generally decreases with increasing wavelength due to decrease in the scattering cross section. For high-resolution spectral measurements the effect may be noticeable. Depending on the application, RRS thus needs to be quantified and possibly corrected for. Of special interest is the effect of RRS in the O_2-A (759-769 nm) and O_2-B (686-697 nm) bands. The O_2-A band is routinely used for retrieval of cloud information. Future satellite missions will use this band in connection with measurements of CO_2. Both the O_2-A and B bands are suitable for measuring fluorescence.

In the near infrared inclusion of RRS in radiative transfer models is computationally challenging due to the high number of atmospheric absorption lines. Sioris and Evans (2000) made the first simulations of RRS in the O_2-A band. They concluded that RRS had a significant affect on line depths at high solar zenith angles in the absence of clouds. Later, Sioris et al. (2003) studied the filling-in of Fraunhofer lines by plant fluorescence. Recently, Joiner et al. (2011) stated that RRS may be have an impact on observations of terrestrial chlorophyll fluorescence by the Japanese Greenhouse gases Observing SATellite (GOSAT).

Sioris and Evans (2000) investigated other types of inelastic scattering that may contribute to filling-in. They concluded that Brillouin scattering is "a minor contributor to the Ring effect in the O_2-A band regardless of viewing geometry". Also the temperature dependence of the Ring effect is "negligible for the limited range of temperatures in the Earth's atmosphere". The filling-in due to atmospheric vibrational Raman scattering (VRS) has been estimated for the 866 nm Calcium II Fraunhofer line by Joiner et al. (2012) and found to be small ($<0.02\%$ for solar zenith angles less then $60°$).

Here, the effect of RRS is studied for the present and future satellite instruments listed in Table 1. Spectra with and without RRS are calculated and the filling-in is quantified for various

Table 1: Some present and future satellite instruments that covers the O_2-A and/or O_2-B band.

Instrument	Spectral range (nm)	FWHM (nm)	Platform
Carbon Monitoring Satellite (CarbonSat)	758-772	0.03	
Fluorescence Imaging Spectrometer (FLORIS)	500-780	0.3-3	FLEX mission
Medium Resolution Imaging Spectrometer (MERIS)	390-1040 (bands)	2.5-30	Envisat
Ocean Land Colour Instrument (OLCI)	400-1020 (bands)	2.5-40	Sentinel-3

atmospheric conditions. For FLEX/FLORIS fluorescence is also included.

Generally the filling-in due to RRS decreases as aerosol and clouds are introduced. As the spectral resolution increases the RRS signal increases as well. The implications of RRS will depend on the application and the analysis to be performed. It is beyond the scope of this document to investigate the effect of RRS on the various data retrievals in use or planned for the instruments listed in Table 1.

Unless otherwise stated, all simulations shown below were performed with the uvspec tool from the libRadtran radiative transfer package (Mayer and Kylling, 2005). The C version (Buras et al., 2011) of the DISORT radiative transfer equation solver (Stamnes et al., 1988) was used with extensions for including rotational Raman scattering (Kylling et al., 2011). For all simulations 16 streams were used and a pseudo-spherical atmosphere geometry assumed (Dahlback and Stamnes, 1991). The standard DISORT solver does not include a fluorescence source. For the simulations of the FLEX mission a fluorescence source was added to the C version of DISORT as described in Appendix A.

2 CarbonSat

The primary mission objective of CarbonSat is the "quantification and monitoring of CO_2 and CH_4 sources and sinks at the regional scale for i) a better understanding of the processes that control the Carbon Cycle dynamics and ii) an independent estimate of local greenhouse gas emissions (fossil fuel, geological CO_2 and CH_4, etc.) in the context of international treaties" (Buchwitz et al., 2010). To measure CO_2 and CH_4 knowledge about the O_2 column is required. This may be obtained by measuring in the strongly absorbing O_2-A band. At high spectral resolution, rotational Raman scattering effects may be present. These effects are quantified for CarbonSat below.

Buchwitz et al. (2010) presents O_2-A band simulations for worst, nominal and best atmospheric cases (their Table 6 and repeated in Table 2). For these cases top of the atmosphere (TOA) nadir

Table 2: Description of CarbonSat cases for radiance simulations.

Case	Solar zenith angle	Surface albedo
Worst case (WC)	75°	0.03
Nominal case (NC)	50°	0.10
Best case (BC)	0°	1.00

radiances are simulated. The worst case is reproduced with the libRadtran/uvspec radiative transfer model in Fig. 1. The best and nominal cases are presented in appendix B. It is noted that the nadir radiances presented by Buchwitz et al. (2010) in their Figs. 20, 25 and 29 have been scaled by $1/\cos(sza)$. Thus, the absolute values presented here and by Buchwitz et al. (2010) differs by factors of 1.0, 0.64 and 0.26 for the best, nominal and worst cases respectively. It is noted that the ambient atmosphere is not defined in Buchwitz et al. (2010). Here the US-standard atmosphere is used (Anderson et al., 1986). The O_2 absorption line structure was
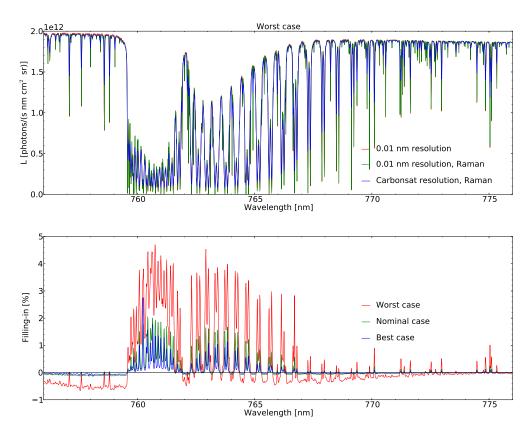
Figure 1: Upper plot: The TOA nadir radiance for the nominal cases as defined by Buchwitz et al. (2010). The red line is a high-resolution (0.01 nm) simulation excluding RRS. The green line is at the same resolution and includes RRS. The blue line is the 0.01 nm resolution RRS simulation convolved with a triangular instrument slit function with FWHM of 0.03 nm. Lower plot: The filling-in for the worst, nominal and best cases as defined by Buchwitz et al. (2010).

calculated by the ARTS-model (Eriksson et al., 2011). In addition to O_2-absorption, the H_2O continuum was included.

The uvspec simulations were made with a spectral resolution of 0.01 nm. The extra-terrestrial solar spectrum was taken from the revised high-resolution Kurucz solar spectrum (Kurucz, 1992; Fontenla et al., 1999) using the "Solar source function" of Clough et al. (2005). Following Chance and Spurr (1997) the spectrum was resampled at even 0.01 nm increments using a triangular filter with full-width at half-maximum (FWHM) of 0.01 nm.

In their Fig. 17 Buchwitz et al. (2010) present the effect of changing the albedo by +10%, the aerosol content by +5% between 0-3 km and by +10% between 3-10 km. They also show what happens if the O_2 concentration increases by 1%. In Fig. 2 the effects of changing the albedo and the aerosol content are shown as calculated with the libRadtran model. Changing the albedo by 10% from 0.1 to 0.11 produced a much larger effect than reported by Buchwitz et al. (2010). A change from 0.1 to 0.101 produced values of a similar magnitude to that shown by Buchwitz et al. (2010) and it is the corresponding change that is shown by the blue line in Fig. 2. No aerosols were included in the albedo sensitivity simulations.
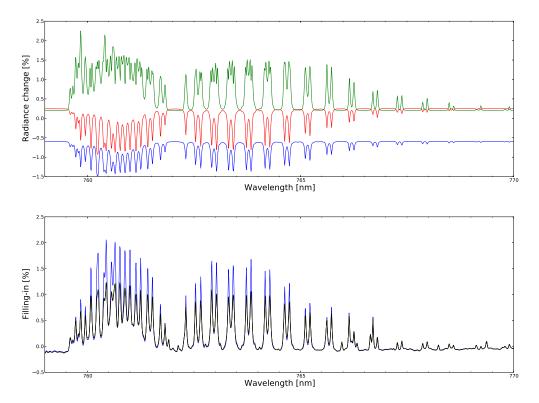
Figure 2: Upper plot: The change in TOA nadir radiances due to an increase in the surface albedo of 1% (blue line); an increase in the aerosol amount of 5% between 0-3 km (red line); and an increase in the aerosol content of 20% between 3-10 km (green line). Note that the lines are offset. Lower plot: The filling-in for the various aerosol (black, red and green lines, all on top of each other) and albedo situations (blue line). See text for details.

It is not known which aerosol model that was used by Buchwitz et al. (2010). Here the aerosol optical depth profile is taken from Elterman (1968). The aerosol type is assumed to be rural background summer and the visibility is set to 10.0 km. For the sensitivity simulations the aerosol optical depth was increased by 5% in the 0-3 km interval and by 20% in the 3-10 km interval. The results are similar to those obtained by Buchwitz et al. (2010).

The lower plot of Fig. 2 shows the filling-in factor for the standard aerosol profile and the cases with increased aerosol amounts (red, standard; green, +5% 0-3 km; and black, +20% 3-10 km, lines). The results are similar for all aerosol situations and the lines are on top of each other. The filling-in for the albedo change case (blue line) is slightly larger than for the aerosol loaded cases. It is similar to the filling-in for the nominal case in Fig. 1.

Both the O_2 absorption lines and the Fraunhofer lines in the extraterrestrial spectrum may be filled in due to RRS. In places the O_2 absorption lines and the Fraunhofer lines overlap. The contribution of the Fraunhofer lines were quantified by performing simulations for the nominal case were the extraterrestrial spectrum was set to unity for all wavelengths. The resulting filling-in, green line Fig. 3, includes only the filling-in of of O_2 absorption lines due RRS. The red line includes filling-in of both the O_2 absorption lines and the Fraunhofer lines.
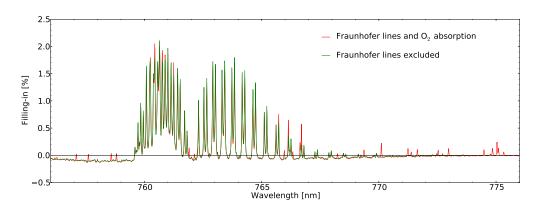
Figure 3: The filling-in of both the O_2 absorption lines and the Fraunhofer lines (red line) and the O_2 absorption lines only (green line).

3 FLORIS/FLEX

The FLEX mission is devoted to monitor the photosynthetic activity of the terrestrial vegetation layer (Drusch and FLEX team, 2011). The natural fluorescence signal is weak compared to the reflected solar radiation. However, by measuring at wavelengths where the solar spectrum is attenuated, for example the O_2-A and B bands, information about natural fluorescence may be retrieved (Guanter et al., 2010). The influence of fluorescence magnitude, surface pressure, aerosol optical depth, aerosol layer height and aerosol type on the TOA radiance, has been investigated by Guanter et al. (2010) for the O_2-A and B bands. Here, the effect of RRS is investigated for a case corresponding to the aerosol free case studied by Guanter et al. (2010). Aerosols generally will decrease the filling-in effect due to RRS.

The TOA radiance in the spectral region covering the O_2-A and B bands, is shown in Fig. 4 at high spectral resolution, 0.01 nm (blue line), for a cloudless sky together with a 0.3 nm
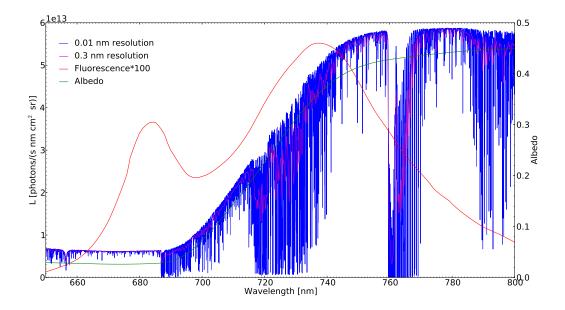

Figure 4: The TOA radiance at high, 0.01 nm (blue line), and coarser, 0.3 nm (magenta line), spectral resolution. The fluorescence spectrum, multiplied by a factor of 100, is shown in red while the surface albedo used for the simulation is shown by the green line. The solar zenith angle is 30°

resolution (red line) calculation representative for the FLORIS instrument. The simulations included fluorescence as shown by the red line. The surface albedo is shown by the green line. The albedo and fluorescence spectra were taken from data generated by the FLUSS project, see also Miller et al. (2005), with the following parameters: Chlorophyll a and b 40; Stoichiometry 1; Fluorescence 0.02; Relative azimuth angle 40; Viewing zenith angle 41.4; Leaf are index 3; Soil-type code 2; Solar zenith angle 30.

The US-standard atmosphere model was adopted (Anderson et al., 1986). The ARTS-model by Eriksson et al. (2011) was used to calculate high-resolution absorption optical depth profiles including O_2, H_2O, CO_2, O_3, CO and CH_4. Most of the absorption line structures are due to H_2O except for the O_2-A and B bands.

Simulations were made with and without RRS and with and without fluorescence. The resulting spectra in the O_2-A and B bands are shown in upper plots of Figs. 5 and 6 respectively. The corresponding filling-in is shown in the lower plots. The fluorescence signal (Upper plots
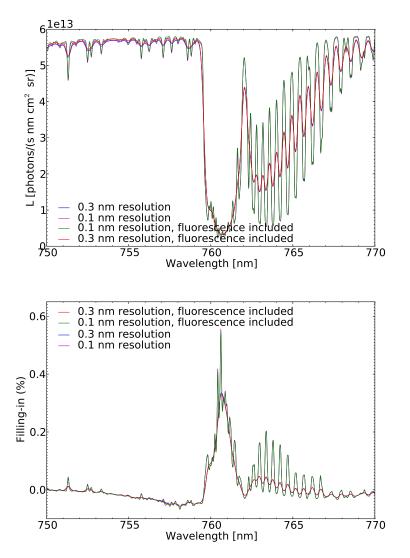

Figure 5: Upper plot: The TOA radiance in the O_2-A band at various spectral resolutions with and without fluorescence. Lower plot: The filling-in due to RRS at various spectral resolutions with and without fluorescence.

Figs. 5 and 6) is stronger in the O_2-B band than in the O_2-A band, see also Figs 2 and 3 in Guanter et al. (2010). The effect due to changes in fluorescence magnitude, surface pressure, aerosol optical depth, aerosol layer height and aerosol type as reported by Guanter et al. (2010), is about an order of magnitude larger than the filling-in caused by RRS.
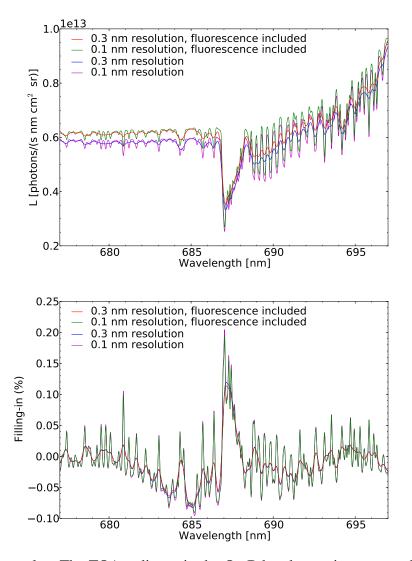
Figure 6: Upper plot: The TOA radiance in the O_2-B band at various spectral resolutions with and without fluorescence. Lower plot: The filling-in due to RRS at various spectral resolutions with and without fluorescence.

Generally an increase in the surface albedo will decrease the absolute magnitude of the filling-in due to the corresponding relative decrease in radiation scattered by the atmosphere and increase in surface scattered radiation. In Fig. 7 the 0.1 nm result from Fig. 5 including fluorescence, are reproduced. Also shown is the filling-in calculated from simulations with surface albedos resembling an evergreen needle forest, desert and fresh snow. These simulations do not include fluorescence. The effect of varying the albedo is small, especially when considering that the filling-in is at the sub-percentage level. The albedo effect is similar in absolute magnitude for the O_2-A and B bands. It appears larger in absolute magnitude for the O_2-B band due to the different scales on the y-axis in the upper and lower plot. In a relative sense it is also larger.
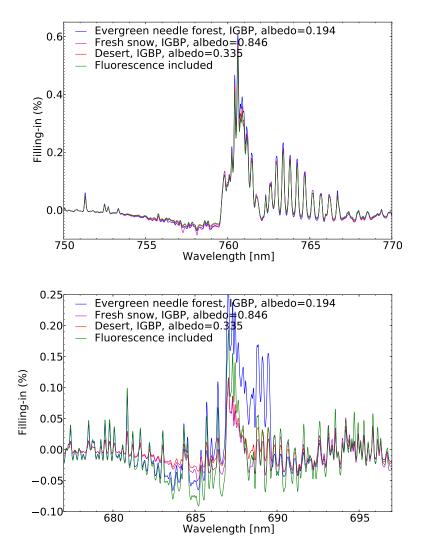
Figure 7: The filling-in due to RRS at 0.1 nm spectral resolution for various surface conditions. Upper plot: The O_2-A band. Lower plot: The O_2-B band.

4   MERIS and OLCI

Both MERIS and OLCI are medium-spectral resolution imaging spectrometers. Both are programmable and operate in the solar reflective spectral range. MERIS has 15 channels. OLCI includes these bands and 6 new ones. The O_2-B band is partly covered by MERIS band 8 which is centered at 681.25 nm and has a band width of 7.5 nm. This is band number 10 for OLCI. The O_2-A band is covered by MERIS band 11 centered at 760.625 nm with band width 3.75 nm. OLCI has bands centered at 761.25, 764,375 and 767.5 nm with band widths of 2.5, 3.75 and 2.5 respectively.

The spectral response functions for the MERIS bands were obtained from `envisat.esa.int/handbooks/meris/CNTR.htm`. For the OLCI bands a Gaussian band shape was assumed with the FWHM set equal to the band widths. The channels relevant for the O_2-A and B bands are shown in Fig. 8.
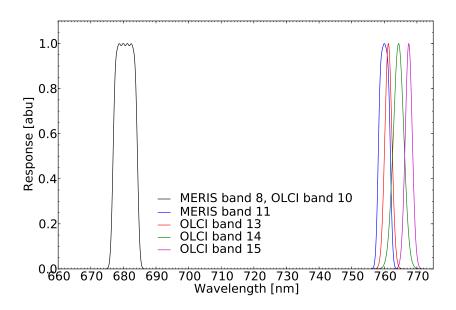

Figure 8: The MERIS and OLCI spectral response functions covering the O_2-A and B bands. See text for further details.

As the spectral resolution decreases the impact of RRS is expected to get smaller. Thus, simulations for the CarbonSat worst case, Table 2, were performed between 673-687 and 755-775 nm with and without RRS. The resulting spectra were convolved with the MERIS and OLCI spectral response functions. The simulated values with and without RRS and the corresponding filling-in is given in Table 3. For the O_2-B band the impact of RRS is minimal. The impact for the various channels in the O_2-A band varies between -0.2% and 0.55%. The variation with solar zenith angle for the various channels in the O_2-A band is shown in Fig. 9.

To illustrate why the magnitude in the filling-in is different for the various bands the filling-in was calculated as a function of wavelength for various solar zenith angles. The simulations

Table 3: Simulated MERIS and OLCI instrument responses for the Carbonsat worst case with and with out RRS.

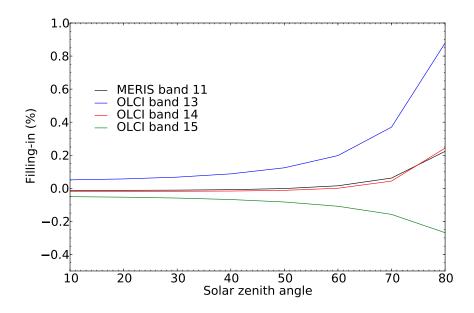| Band	Without RRS photons/(cm² nm s)	Including RRS photons/(cm² nm s)	Difference (%)
MERIS band 8	2.49838517e+12	2.49730222e+12	-0.04
MERIS band 11	7.96578743e+11	7.97510315e+11	0.11
OLCI band 13	5.47955435e+11	5.50991181e+11	0.55
OLCI band 14	8.49684702e+11	8.50567839e+11	0.10
OLCI band 15	1.53577668e+12	1.53269297e+12	-0.20

Figure 9: The filling-in as a function of solar zenith angle under cloudless conditions for the MERIS band 11 and the OLCI band 13-15 channels.

were made at GOME spectral resolution with FWHM of 0.35 nm and a Gaussian slit function. The surface albedo was set to zero. The resulting filling-in spectra are shown in Fig.10. The spectral location of the various MERIS and OLCI bands, Fig. 8, explains the various magnitudes of the filling-in for the different bands. Note that the absolute magnitude of the filling-in for GOME-resolution will be larger then for the relatively broad bands of MERIS and OLCI.

For satellite geometries maximum filling-in are found for cloudless skies. The effect on the filling-in due to aerosols and clouds are shown in Figs. 11 and 12, respectively.
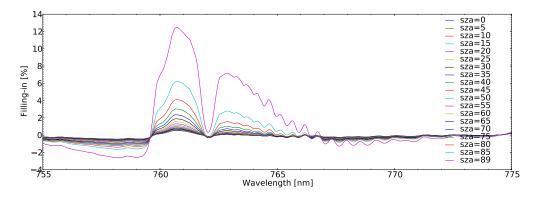
Figure 10: The filling-in calculated for various solar zenith angles at GOME instrument resolution (FWHM 0.35 nm) for a cloudless sky.
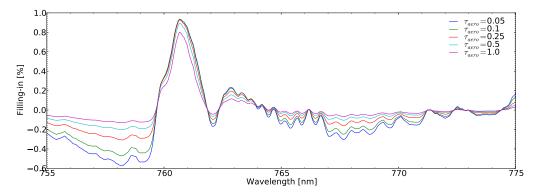

Figure 11: The filling-in for various aerosol loads for a solar zenith angle of $50°$. The spectral resolution is as in Fig 10.

5   Conclusions

The effect of rotational Raman scattering has been investigated for the CarbonSat, FLEX/FLORIS, MERIS and OLCI instruments. Generally the effect of RRS decreases with decreasing spectral resolution. Also, the presence of clouds and aerosol decrease the impact of RRS. The importance of RRS will depend on the retrieval procedure adopted for the quantity to be measured. Retrieval procedures that utilize the full spectral resolution of CarbonSat and FLEX/FLORIS will most likely benefit from including RRS. Radiative transfer models may calculate the impact of RRS for these instruments. Thus, corrections for RRS may readily be included in the retrieval and potentially reduce the uncertainty in the retrieved quantity. It is noted that for high-resolution CarbonSat measurements over the ocean, vibrational Raman scattering may have an additional filling-in effect.
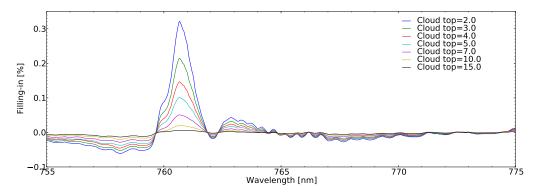
Figure 12: The filling-in for various cloud top heights for a solar zenith angle of 50°. The cloud had an optical depth of 10 and the effective droplet radius was 10 μm. The spectral resolution is as in Fig 10.

References

Anderson, G., Clough, S., Kneizys, F., Chetwynd, J., and Shettle, E.: AFGL atmospheric constituent profiles (0-120 km), *Tech. Rep. AFGL-TR-86-0110*, Air Force Geophys. Lab., Hanscom Air Force Base, Bedford, Mass., 1986.

Buchwitz, M., Bovensmann, H., Reuter, M., Geilowski, K., and Burrows, J. P.: Carbon Monitoring Satellite - CarbonSat, Mission Requirements Document (MRD), Tech. Rep. IUP-CS-MRD-0001, Version 3.2, IUP, University of Bremen, 2010.

Buras, R., Dowling, T., and Emde, C.: New secondary-scattering correction in DISORT with increased efficiency for forward scattering, J. Quant. Spectrosc. Radiat. Transfer, 112, 2028–2034, 2011.

Chance, K. and Spurr, R. J. D.: Ring effect studies: Rayleigh scattering including molecular parameters for rotational Raman scattering, and the Fraunhofer spectrum, Appl. Opt., 36, 5224–5230, 1997.

Clough, S. A., Shephard, M. W., Mlawer, E. J., Delamere, J. S., Iacono, M. J., Cady-Pereira, K., Boukabara, S., and Brown, P. D.: Atmospheric radiative transfer modeling: a summary of the AER codes, J. Quant. Spectrosc. Radiat. Transfer, 91, 233–244, 2005.

Dahlback, A. and Stamnes, K.: A new spherical model for computing the radiation field available for photolysis and heating at twilight, Planet. Space Sci., 39, 671–683, 1991.

Drusch, M. and FLEX team: FLEX Candidate Earth Explorer Mission: Mission Requirements Document (MRD), Tech. Rep. EOP-SM/2221/MDr-md, European Space Agency, 2011.

Elterman, L.: UV, visible, and IR attenuation for altiutdes to 50 km, Air Force Cambridge Research Laboratories, Environmental Research Papers No. 285, Bedford, Mass., 56 pp, 1968.

Eriksson, P., Buehler, S. A., Davis, C. P., Emde, C., and Lemke, O.: ARTS, the atmospheric radiative transfer simulator, version 2, J. Quant. Spectrosc. Radiat. Transfer, 112, 1551–1558, 2011.

Fontenla, J., White, O. R., Fox, P. A., Avrett, E. H., and Kurucz, R. L.: Calculation of solar irradiances. I. Synthesis of the solar spectrum, The Astrophysical Journal, 518, 480–499, 1999.

Guanter, L., Alonso, L., Gómez-Chova, L., Meroni, M., Preusker, R., Fischer, J., and Moreno, J.: Developments for vegetation fluorescence retrieval from spaceborne high-resolution spectrometry in the O_2-A and O_2-B absorption bands, J. Geophys. Res., 115, 2463–2479, doi:doi:10.1029/2009JD013716, 2010.

Joiner, J., Yoshida, Y., Vasilkov, A. P., Yoshida, Y., Corp, L. A., and Middleton, E. M.: First observations of global and seasonal terrestrial chlorophyll fluorescence from space, Biogeosciences, 8, 637–651, http://www.biogeosciences.net/8/637/2011/, 2011.

Joiner, J., Yoshida, Y., Vasilkov, A. P., Middleton, E. M., Campbell, P. K. E., Yoshida, Y., Kuze, A., and Corp, L. A.: Filling-in of far-red and near-Infrared solar lines by terrestrial and atmospheric effects: simulations and space-based observations from SCIAMACHY and GOSAT, Atmos. Meas. Tech. Discuss., 5, 163–210, doi:10.5194/amtd-5-163-2012, http://www.atmos-meas-tech-discuss.net/5/163/2012/, 2012.

Kurucz, R. L.: Synthetic infrared spectra, in: Infrared Solar Physics, edited by Rabin, D. and Jefferies, J., IAU Symp. 154, Kluwer, Acad., Norwell, MA, 1992.

Kylling, A., Mayer, B., and Blumthaler, M.: Technical Note: A new discrete ordinate first-order rotational Raman scattering radiative transfer model, implementation and first results, Atmos. Chem. Phys., 11, 10 471–10 485, doi:10.5194/acp-11-10471-2011, http://www.atmos-chem-phys.net/11/10471/2011/, 2011.

Mayer, B. and Kylling, A.: Technical note: the libRadtran software package for radiative transfer calculations-description and examples of use, Atmos. Chem. Phys., 5, 1855–1877, 2005.

Miller, J. R., Berger, M., Goulas, Y., Jacquemond, S., Lous, J., Moise, N., Mohammed, G., Moreno, J., Moya, I., Pedrós, R., Verhoef, W., and Zarco-Tejada, P. J.: Development of a Vegetation Fluorescence Canopy Model, Final Report, Tech. rep., ESTEC Contract No. 16365/NL/FF, 2005.

Sioris, C. E. and Evans, W. F. J.: Impact of rotational Raman scattering in the $O_2 A$ band, Geophys. Res. Lett., 27, 4085–4088, 2000.

Sioris, C. E., Courrèges-Lacoste, G. B., and Stoll, M.-P.: Filling in of Fraunhofer lines by plant fluorescence: Simulations for a nadir-viewing satellite-borne instrument, J. Geophys. Res., 108, doi:10.1029/2001JD001 321, 2003.

Stamnes, K., Tsay, S.-C., Wiscombe, W., and Jayaweera, K.: Numerically stable algorithm for discrete–ordinate–method radiative transfer in multiple scattering and emitting layered media, Appl. Opt., 27, 2502–2509, 1988.

A   Inclusion of fluorescence in libRadtran/uvspec/cdisort

Fluorescence may be treated as a re-emission of radiation and not as a scattering process. The lifetimes of the fluorescence processes are assumed to be sufficient for the emitted photon to loose all memory of the direction of the incoming photon. Thus the re-emitted photon are re-emitted isotropically.

The radiative transfer equation are solved with the following bottom boundary condition (Stamnes et al., 1988, Eq: 11b)

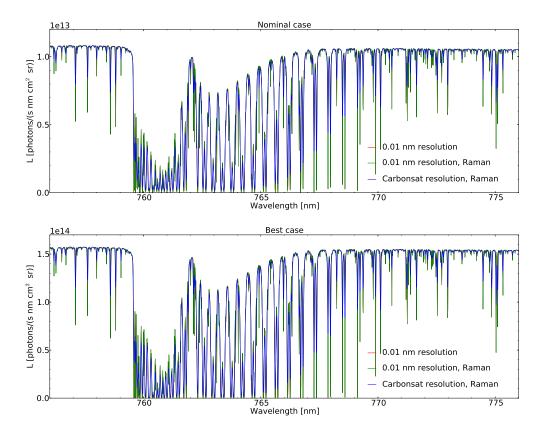$$u(\tau = \tau_L, +\mu, \phi) = u_g(\mu, \phi). \tag{1}$$

For fluorescence the radiance u_g leaving the bottom boundary is

$$u_g(\mu, \phi) = F \tag{2}$$

where F is the fluorescence source in the same units as the incoming solar flux at the top of the atmosphere (for example mW/(m^2 nm sr)). Additional surface bidirectional reflection of radiation may also be included.

The fluorescence source at the bottom boundary has been included in the C version (Buras et al., 2011) of the DISORT radiative transfer model. Furthermore, the uvspec tools has been extended with two options that allows the user to either include fluorescence that is constant with wavelength or a wavelength dependent fluorescence spectrum.

B   CarbonSat

Simulations by libRadtran/uvspec of the best and nominal cases for CarbonSat.

Figure 13: The TOA nadir radiance for the nominal and best cases as defined by Buchwitz et al. (2010). Green lines are high-resolution (0.001 nm) simulations. The red lines are 0.01 nm resolution simulations that have been convolved with a triangular instrument slit function with FWHM of 0.03 nm. The black lines are similar to the red lines, but include rotational Raman scattering.

REPORT SERIES SCIENTIFIC REPORT	REPORT NO. OR 10/2012	ISBN: 978-82-425-2487-4 (print) 978-82-425-2488-1 (electronic) ISSN: 0807-7207	
DATE MARCH 2012	SIGN.	NO. OF PAGES 18	PRICE NOK 150.-
TITLE Rotational Raman scattering in the O2-A and O2-B bands: Simulations for Carbonsat, FLEX/FLORIS, MERIS and OLCI		PROJECT LEADER Arve Kylling	
		NILU PROJECT NO. O-111081	
AUTHOR(S) Arve Kylling		CLASSIFICATION * A	
		CONTRACT REF. ESTEC Contract No. AO/1-6607/10/NL/LvH	
QUALITY CONTROLLER: Kjetil Tørseth			
REPORT PREPARED FOR European Space Agency (ESA)			

ABSTRACT
Rotational Raman scattering (RRS) causes filling-in of absorption lines in Earth shine spectra. It is routinely accounted for in analysis of UV and visible spectra measured both by satellite and ground-based instruments. RRS is also present at longer wavelengths, however, the magnitude generally decreases with increasing wavelength due to decrease in the scattering cross section. For high-resolution spectral measurements the effect may be noticeable. Depending on the application, RRS thus needs to be quantified and possibly corrected for. Of special interest is the effect of RRS in the O_2-A (759-769 nm) and O_2-B (686-697 nm) bands. Here, the effect of RRS in these bands is studied for the present and future satellite instruments CarbonSat, FLEX/FLORIS, MERIS and OLCI.

NORWEGIAN TITLE		
Rotasjonell Raman spredning i O_2-A og O_2-B bandene: Simuleringer for CarbonSat, FLEX/FLORIS, MERIS og OLCI		

KEYWORDS		
Remote sensing	Radiative transfer	Atmosphere and climate

ABSTRACT (in Norwegian)
Absorpsjonslinjer i solspektra fylles igjen på grunn av rotasjonell Raman spredning (RRS). Ved analyse av UV og synlige spektra blir RRS rutinemessig korrigert for. Effekten er også tilstede ved lengre bølgelengder, men generelt avtar den når bølgelengdene øker. For spektra med høy spektraloppløsning kan effekten være av betydning. Avhengig av anvendelsen kan det være nødvendig å kvantifisere og korrigere for RRS også ved lengre bølgelengder. Av spesiell interesse er effekten i O_2-A (759-769 nm) og O_2-B (686-697 nm) bandene. Effekten av RRS i disse bandene blir presentert for satellittinstrumentene CarbonSat, FLEX/FLORIS, MERIS og OLCI.

* Classification   *A*   *Unclassified (can be ordered from NILU)*
                        B   *Restricted distribution*
                        C   *Classified (not to be distributed)*

NILU – Norwegian Institute for Air Research is an independent, nonprofit institution established in 1969. Through its research NILU increases the understanding of climate change, of the composition of the atmosphere, of air quality and of hazardous substances. Based on its research, NILU markets integrated services and products within analyzing, monitoring and consulting. NILU is concerned with increasing public awareness about climate change and environmental pollution.